Post-Print

When citing this work, cite the original published paper.

EXPERIMENTAL INVESTIGATION ON THE AERODYNAMIC INTERACTION BETWEEN A HELICOPTER AND GROUND OBSTACLES

G. Gibertini, D. Grassi, C. Parolini, D. Zagaglia*, A. Zanotti

Politecnico di Milano, Dipartimento di Scienze e Tecnologie Aerospaziali

Campus Bovisa, Via La Masa 34, 20156 Milano, Italy

*Corresponding author. e-mail: daniele.zagaglia@polimi.it

Abstract:

In the present study, experiments were performed to investigate the aerodynamic interaction between a helicopter and ground obstacles. A new experimental setup was realised and validated. The motorised helicopter model, which included the fuselage, was positioned in different positions relative to a model building in order to replicate different hovering configurations. The use of a helicopter model with a six-component balance and a building model with several pressure taps allowed a database to be compiled for the loads on the helicopter and obstacle. First several tests were performed without the building in order to develop a reference database and assess the experimental setup through a comparison with results in the literature. The measured loads were analysed to investigate the interference effects of the building model on the helicopter performance. A physical interpretation of the flow phenomena was obtained through analysis of the obstacle pressure measurements and particle image velocimetry surveys of relevant configurations.

Keywords: Rotorcraft, Aerodynamics, Vortex Interaction, Particle Image Velocimetry (PIV), Ground Obstacles.

1 INTRODUCTION

The helicopter is a very versatile flying machine that is often required to operate close to vertical obstacles such as buildings, ships and mountain walls. The danger intrinsic to these flight conditions is evident in the accident database [1] collected by the Joint Helicopter Safety Analysis Team (JHSAT) for the International Helicopter Safety Team (IHST). This study highlighted the fact that most helicopter accidents (61.4%) occur during take-off and landing – i.e. generally in the presence of ground obstacles. These situations can be further complicated under windy conditions, particularly when the helicopter flies inside the turbulent and extremely unsteady wake generated by an obstacle [2].

1

Therefore, the aerodynamic interaction between a helicopter and obstacles is a quite important research subject, and several numerical and experimental studies have been published in the scientific literature. The most commonly investigated situation in the recent literature has been the helicopter in proximity to ship decks.

For instance, Crozon et al. [3] analysed different numerical approaches for the simulation of rotors flow field in a ship air wake, while Alpman et al. [4] were able to fully couple Computational Fluid Dynamics (CFD) simulations with flight dynamics for the study of similar configurations.

Lee and Zan [6, 7] and Zan [8] performed experiments to measure the loads acting on a helicopter in the wake of a scaled frigate for different configurations: isolated rotor, isolated fuselage, and rotor with fuselage. Timm [5] was the first to observe the flow recirculation induced by the interaction between the rotor and obstacle through flow visualizations. Recently, the use of particle image velocimetry (PIV) has enabled the quantitative analysis of this interacting flow field; for example Nacakli and Landman [9] examined the interaction between a helicopter and the air wake of a frigate. Rajagopalan et al. [10] and Quinliven and Long [11] compared numerical and experimental results for the topology of the interacting flow field using scaled models of helicopter and buildings. In contrast, Polsky and Wilkinson [12] compared the results of a numerical study with those of an experiment on a full-scale helicopter in the proximity of a hangar.

Despite the relative abundance of numerical and experimental works, a systematic study of the aerodynamic phenomena involved which considers a wide set of cases is lacking. Moreover, most of these investigations have focused on the effect on the helicopter performance and handling qualities, and *de facto* have neglected the corresponding load effects on the obstacle.

This paper presents the results of a series of tests reproducing hovering flight conditions at different positions with respect to a simplified volume with a parallelepiped shape. This parallelpiped model was courteously made available by DLR in the frame of a collaboration that should continue in the future under the auspices of the GARTEUR organisation [13]. Scale effects were unavoidably present in the experiment compared to similar full-scale conditions; however the scaled-down tests were essential for producing an accurate and repeatable database, because laboratory conditions are much more stable and controllable. Measurement of both the loads acting on the rotor and the pressure distributions over the external surfaces of the obstacle revealed information on the mutual effects of the aerodynamic interaction. PIV was used to investigate the details of the interacting flow field under several conditions of interest.

2 EXPERIMENTAL SET UP

The test rig essentially consisted of a helicopter model, inspired by the MD-500, and a geometric obstacle which represented an ideal building. The helicopter model was held by a horizontal strut fixed to a system of two

motorised orthogonal sliding guides to allow the relative position to be changed with respect to the obstacle along the vertical and longitudinal directions of the fuselage. Figure 1 shows the set up of the helicopter–building interaction experiment as well as the reference system used in the present study. For the coordinate reference system, the X-Z plane was aligned with the mid-span plane of the building model and the X-Y plane was aligned with the floor. The origin of the reference system was located on the floor, at the mid-span of the front face. As shown in Figure 4, the Y axis lay on the longer side of the building base.
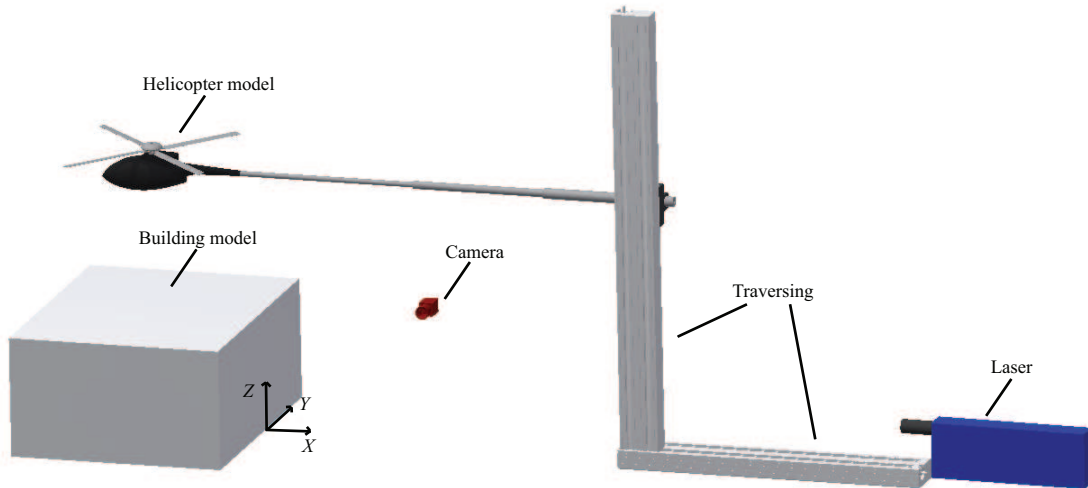

Figure 1: Layout of helicopter–building interaction experiment and reference system (including PIV set up).

2.1   Helicopter model

Figure 2 shows the helicopter model (rotor and fuselage). The rotor had four untwisted and untapered rectangular blades with a chord of $c = 0.032$ m and radius of $R = 0.375$ m, at a $1 : 10.7$ scale ratio. The NACA 0012 airfoil was used. No swash plate was present, so the blade pitch angle was fixed to $10°$. A rotational speed of 2480 rpm was maintained during all the tests by means of a brush-less low-voltage electrical motor with an electronic controller. The resulting Mach number and Reynolds number at the blade tip were $M_{\mathrm{TIP}} = 0.286$ and $Re_{\mathrm{TIP}} = 214{,}000$, respectively.

The forces and moments acting on the rotor were measured with a six-component balance nested inside the fuselage. A Hall effect sensor produced one signal per revolution to act as the feedback signal for RPM control. Figure 3 shows a schematic of the helicopter model layout.

The fixed rotor described above does not represent all of the details of the complex phenomena which occur in an articulated rotor, e.g. the flapping motion. However, in the present experiment the model was kept in a fixed position (hovering flight); therefore, the forward flight effects that strongly affect blade flapping were not present. Hence, the behaviour of the interaction between the helicopter model and the obstacle can be considered adequately representative of a general case. The choice of a fixed rotor was also motivated by the intention of obtaining well-defined reference data for comparison with numerical simulations.

With regard to the inexact matching of M_{TIP}, the aim of the present study was to analyse the interaction between the rotor wake and obstacle; therefore, matching Mach number at tip was not essential, because the topology of the wake is not greatly influenced by such a parameter ([14],[15]). A larger effect of the small-scale can be expected because of the low Re_{TIP}. At low Reynolds numbers, the blade profile drag coefficient increases; this produces an higher resistant torque, which results in a swirl stronger than in full-scale condition. Nevertheless note that the employed model was able to reach a Reynolds number higher than the one achieved in similar investigations by [10] and [11], and practically equal to that obtained by [6]. The model dimensions were limited by the need to avoid interference by the surrounding test environment.

2.2 Building model

The building model was a parallelepiped with sharp edges; it comprised an internal structure of aluminium alloy square tubes holding external aluminium alloy plates. The dimensions of the parallelepiped were 0.45 m × 0.8 m × 1.0 m. The building model was equipped with 150 pressure taps (see Fig. 4), of which 31 lay on the top plate , 21 lay on the side plate and 48 lay on the front plate. The remaining taps were located on the other three faces, which were not considered in the present study. The pressures were acquired by means of five 32-port scanners by Pressure System Inc. embedded inside the building model. The declared accuracy of these pressure transducers led to an uncertainty in pressure coefficients of ± 0.15, but previous experience and some tests carried out before the experiment led to a C_p uncertainty of less than 0.1.

2.3 PIV set up

The PIV system comprised a Litron NANO-L-200-15 Nd:Yag double-pulse laser with an output energy of 200 mJ and wavelength of 532 nm, and an Imperx ICL-B1921M CCD camera with a 12-bit, 1952 × 1112 pixel array. The laser was positioned on the floor so that the laser sheet was aligned with the X-Z plane (see the layout in
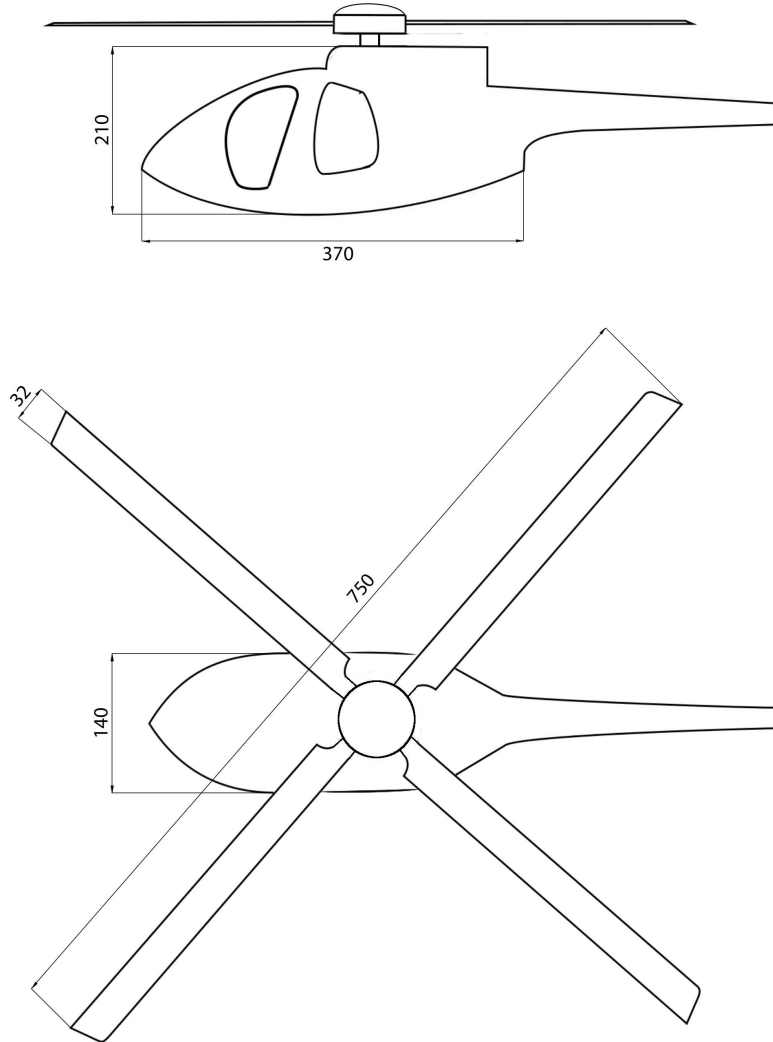
Figure 2: Sketch of helicopter model (dimensions in mm).

Fig. 1). The camera line of sight was positioned perpendicular to the laser sheet. As shown in Figure 5, the PIV measurement window was 300 mm × 400 mm. In order to achieve better resolution of the image pairs, the measurement area comprised two adjacent windows, one on top of the other, with a small overlapping band between them. The synchronisation of the two laser pulses with the image pair exposure was controlled by a six-channel Quantum Composer QC9618 pulse generator. A PIVpart30 particle generator by PIVTEC with Laskin atomizer nozzles was used for the seeding, which consisted of small oil droplets with diameters of 1-2
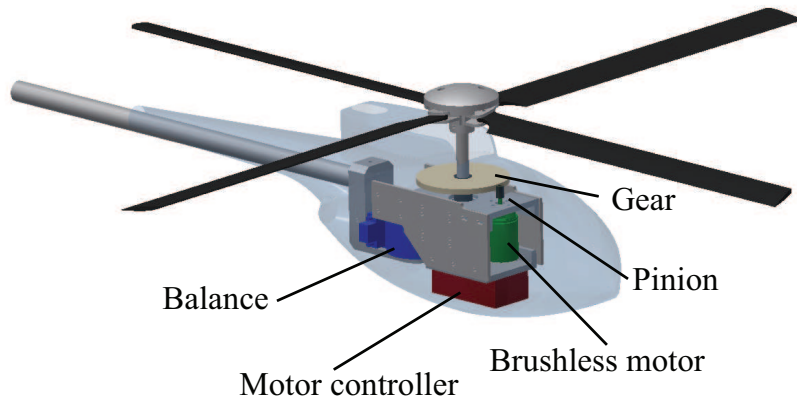
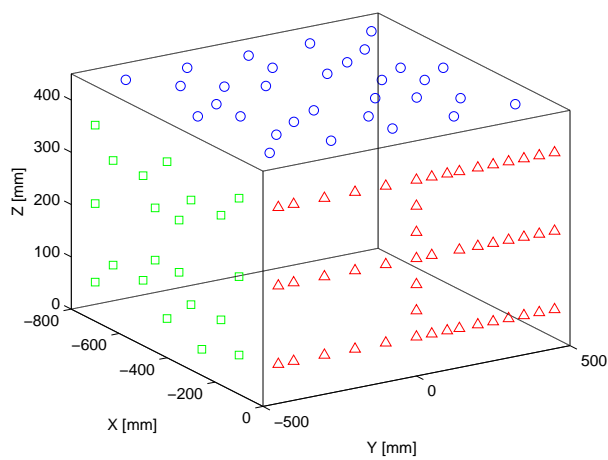Figure 3: Sketch of helicopter model and nested instrumentation.

Figure 4: Pressure tap locations on model building. The top, side and front plates are characterised by circle, square and triangle markers respectively.

μm. The image pair analysis was carried out using PIVviev 2C software [16], which was developed by PIVTEC in close cooperation with the PIV-Groups of DLR.
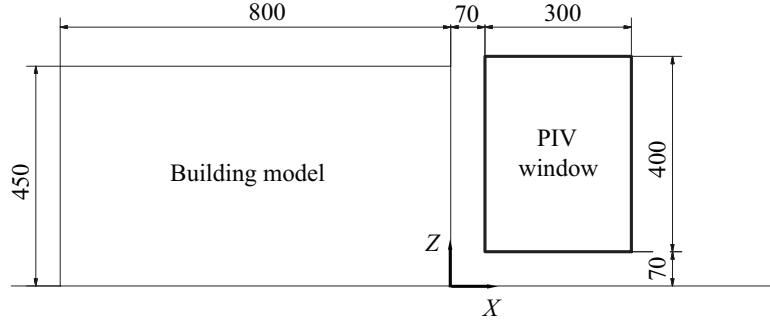
Figure 5: Schematic of PIV measurement area (dimensions in mm).

3 TEST MATRIX AND EXPERIMENTAL PROCEDURE

As mentioned in Section 1, each test comprised a measurement where the model was kept in a defined position with respect to the building model. Thus, the tests essentially reproduced hovering flight conditions (although not exactly trimmed).

Tests were carried out with the parallelepiped leaned on the 0.8 m × 1 m face to represent a low-rise building. With respect to the reference systems shown in Fig. 1, several series of tests consisting of vertical sweeps, where X and Y were constant or horizontal sweeps, where Z and Y were constant, were carried out. Table 1 lists the parameters used for the different test conditions. The coordinates which identify the helicopter model position refer to the intersection point between the rotor shaft axis and rotor disk.

N	Building Configuration		Sweep Axis			First Point			Last Point		
	No Build.	Build.	X	Y	Z	X/R	Y/R	Z/R	X/R	Y/R	Z/R
0	×					·/·	·/·	5	·/·	·/·	5
1	×				×	·/·	·/·	1	·/·	·/·	5
2		×			×	-1.07	0	2	-1.07	0	5
3		×			×	-0.53	-0.67	2	-0.53	-0.67	5
4		×			×	2	0	1	2	0	4.7
5		×	×			-1	0	2	1	0	2

Table 1: Test matrix

In order to reduce the balance thermal drifts, each test point corresponded to a single run where the motor was started from rest and then stopped again at the end of the acquisition. The acquisition took place over 5 s long and was preceded by 10 s of flow stabilisation. The balance zeroes were acquired immediately before and

7

after each run and the mean of these two readings was used to account for the balance thermal drift. However, because of the short run time, this zero drift was quite small. The rotational speed was set equal to 2480 rpm (corresponding to $M_{\text{TIP}} = 0.286$), although drifts of up to 30 rpm occurred during the tests. Thus, the actual RPM value was continuously acquired so that the thrust and torque coefficients would be correctly computed. Four runs were carried out for each measurement point, and the obtained results were averaged.

A similar procedure was adopted for pressure measurements; however the acquisition time was set to 10 s in order to filter out, by averaging over a longer time, the pressure fluctuations due to the unsteadiness. The pressure results were represented by the pressure coefficient C_p:

$$C_p = \frac{P - P_\infty}{\frac{1}{2}\rho V_{\text{IND}}^2}, \tag{3.1}$$

where P_∞ is the far-field pressure and V_{IND} is the estimated rotor-induced velocity according to the Momentum Theory (MT) [17] and is defined as $V_{\text{IND}} = V_{\text{TIP}}\sqrt{\frac{C_{t,OGE}}{2}}$.

4 TEST RESULTS AND DISCUSSION

4.1 Load and pressure measurements

test 0 was intended to be a repeatability test; it consisted of several repetitions of the load measurements with the helicopter model in a fixed position in order to check the precision of the measurement chain. This test was carried out without the building model at a height of $Z/R = 5$, i.e. out of ground effect (OGE) condition. After 30 runs, the average thrust coefficient was $C_{t_{OGE}} = 0.00705$, and the torque coefficient was $C_{q_{OGE}} = 0.000750$. The standard deviation was 0.3% for both the thrust and torque coefficients; thus, the measurement showed a high level of repeatability.

The first sweep in the Z (vertical) direction (test 1 of Table 1) was carried out without obstacles to produce a reference condition for comparison with the obstacle effects. Figure 6(a) plots the results of this reference test in terms of $C_t/C_{t_{OGE}}$ and compares them with those obtained by Fradenburgh [18]. Fradenburgh conducted ground effect tests using a two-bladed rotor, with a diameter of $D = 2ft \simeq 0.6m$ and chord of $c = 2in \simeq 5cm$ operating at V_{TIP} of approximately $600ft/s$, $RPM \simeq 5800$. Despite the difference in geometric and operating conditions, the present results showed good agreement and thus validated the experimental setup. Figure 6(b) presents the results in terms of figure of merit (FM). Under the OGE condition, $FM = 0.564$. This is not far from the typical FM for helicopters and is within the expected order of magnitude for a model of this scale without a blade sweep.

The first test with the building model (test 2) was a vertical sweep along the vertical projection of the roof

(a) Thrust coefficient   (b) Figure of merit
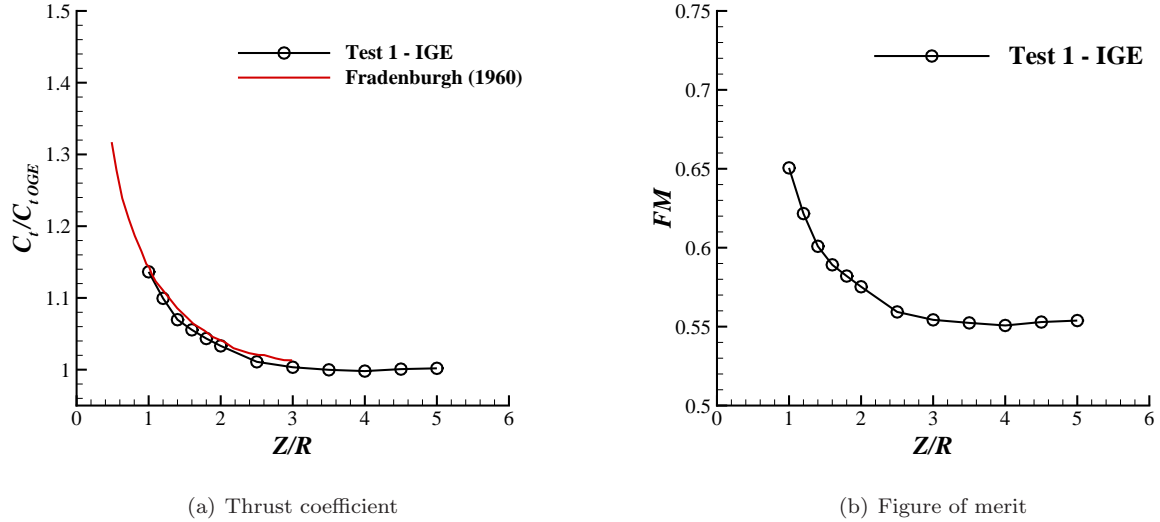
Figure 6: Ground effect test without building model. Results were for different heights from the ground and compared with data from literature

centre; this was an ideal representation of a slow vertical landing on the middle of a flat roof of a low-rise building. For the reference system, this corresponded to different Z values at $X/R = -1.07$ and $Y/R = 0$. In order to more directly compare the roof effect with the ground effect of reference test 1, the results of the roof landing were plotted with a Z offset equal to the building model height. As shown in Fig. 7, the effect of a roof with this extension was practically equal to the ground effect, because the entire wake induced by the rotor impinged on the roof (see pressure contour in Fig. 11a). The high-pressure region corresponding to the impingement area of the rotor wake saw a reduced maximum peak as the helicopter moved away from the obstacle, which implies a reduced ground effect (see Figs. 11c and e). A slight depression was observed on the front face which was washed by the rotor-induced wind.

Test 3 had exactly the same measurement points as test 2 in terms of Z/R, but X and Y were shifted so that the rotor centre lay 25% along the upper surface diagonal. For the reference system, this corresponded to different Z values at $X/R = -0.53$ and $Y/R = -0.67$. As shown in Fig. 8, the results of test 3 presented a deterioration in performance compared to test 2, with lower values of C_t and FM. This ground effect reduction was because part of the rotor projection did not directly lie on top of the building model; hence, part of the induced wake impacted on the ground, which was at a greater distance. This can also be observed in the C_p plots of Figs. 11b, d and f. In test 2 the entire high-pressure region due to the wake impingement was confined to the top of the block; in test 3, part of this area did not directly lie on it. In this case, the rotor-induced wind

9

produced negative pressure coefficients on both the front and lateral faces.

Test 4 represented a landing beside the building, at $X/R = 2$ and $Y/R = 0$. Figure 9 compares the measured thrust coefficients with those of test 1 (without building). A reduction in thrust performance which was even lower than that under OGE condition was present when the rotor arrived at the same height as the building model. This reduction indicates an augmented induced velocity associated with strong recirculation between the building and rotor, as observed by Quinliven and Long [11] in a similar case. These negative effects became negligible from $Z/R = 3$, which was 2.5 times the building height. Overpressures were apparent on the front face, particularly on the lower part of the obstacle where the wake, deflected by the ground, impinged (see Fig. 12).

Test 4 represented a landing beside the building, at $X/R = 2$ and $Y/R = 0$. Figure 9 compares the measured thrust coefficients with those of test 1 (without building). C_t values even lower than those under OGE condition were present when the rotor arrived at the same height as the building model. A partial thrust recovery was obtained at even lower heights when the helicopter interacted with the front face. However the performance drop with respect to the same test without building model concerning the thrust coefficient was even higher, probably indicating an augmented induced velocity associated with strong recirculation between the building and rotor, as observed by Quinliven and Long [11] in a similar case. These negative effects became negligible from $Z/R = 3$, which was 2.5 times the building height. Overpressures were apparent on the front face, particularly on the lower part of the obstacle where the wake, deflected by the ground, impinged (see Fig. 12).

Test 5 considered a set of points on a horizontal line on the symmetry plane at $Z/R = 2$. These points can represent a slow horizontal approach. Figure 10 shows the results for X/R varying from -1 to 1. The first considered position was $X/R = -1$; the entire rotor disk was over the obstacle, although not exactly centred with respect to the building roof (the centre of the roof was at $X/R = -1.07$). For this configuration, $C_t/C_{t_{OGE}} = 1.195$, according to the results of test 2 at the same height. Away from the building centre, $C_t/C_{t_{OGE}}$ decreased according to the minor percentage of the rotor projection lying on top of the building. $C_t/C_{t_{OGE}}$ was 1.03 for the outer position, just as it was in test 1 at the same height. Figure 13 presents the pressure results. The pressure distribution with the model positioned at $X/R = -1$ was substantially equivalent to the results obtained in test 2 at the same height, even if the X position of the helicopter model was slightly different. When the rotor centre lay exactly on the building edge ($X/R = 0$), the pressure distributions on the different faces of the building indicated the presence of a complex flow structure that was markedly asymmetrical. The diagonal pattern on the front face was probably related to the helicoidal structure of the rotor wake. Although the adopted measurement system did not allow a thorough evaluation of the pressure
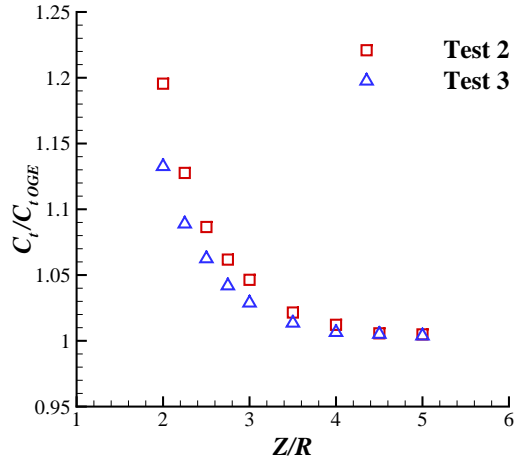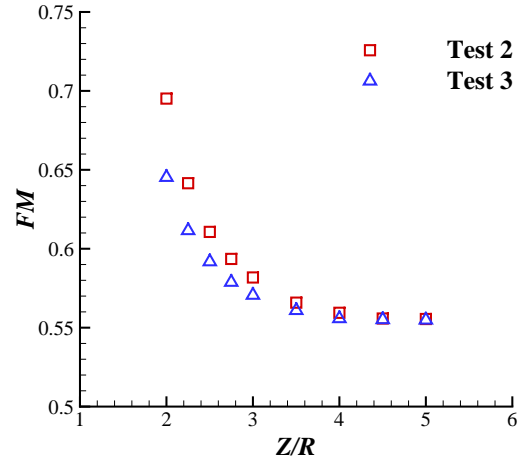
10
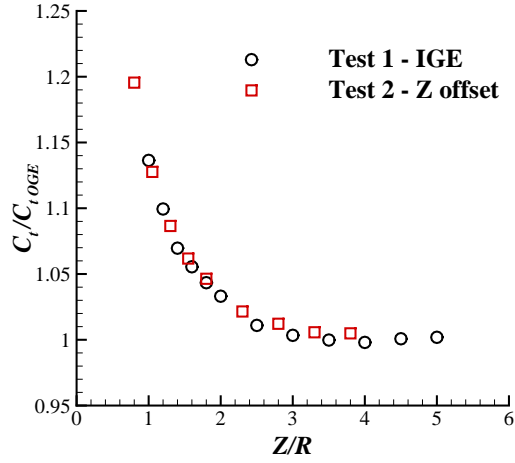
(a) Thrust coefficient
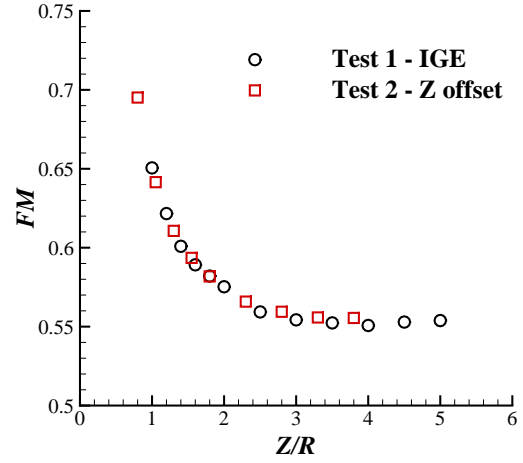
(b) Figure of merit

Figure 7: Comparison of C_t and FM for test 1 (ground effect reference test without building) and test 2 (Ground effect test on building roof centre: $X/R = -1.07$ and $Y/R = 0$). The curve of test 2 has a Z off-set equal to the building model height (0.45 m or $1.2R$).

fluctuations, the single samples acquired on this face presented a higher variability than in all of the other cases. For $X/R = 1$ the helicopter effect was only apparent on the front face, where the overpressure was higher than that in test 4 because of the shorter distance from the obstacle.
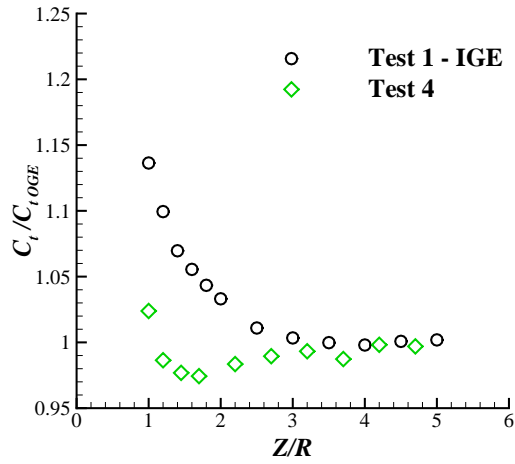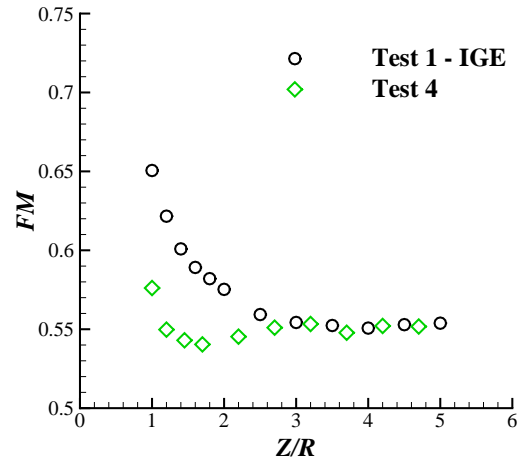
(a) Thrust coefficient

(b) Figure of merit

Figure 8: Comparison of C_t and FM for test 2 (ground effect test on building roof centre: $X/R = -1.07$ and $Y/R = 0$) and test 3 (ground effect test on the building roof: $X/R = -0.53$ and $Y/R = -0.67$). The curves of test 2 and 3 have a Z off-set equal to the building model height (0.45 m or $1.2R$).

(a) Thrust coefficient

(b) Figure of merit

Figure 9: Comparison of C_t and FM for test 1 (ground effect reference test without the building) and test 4 (vertical sweep on side of building: $X/R = 2$ and $Y/R = 0$).
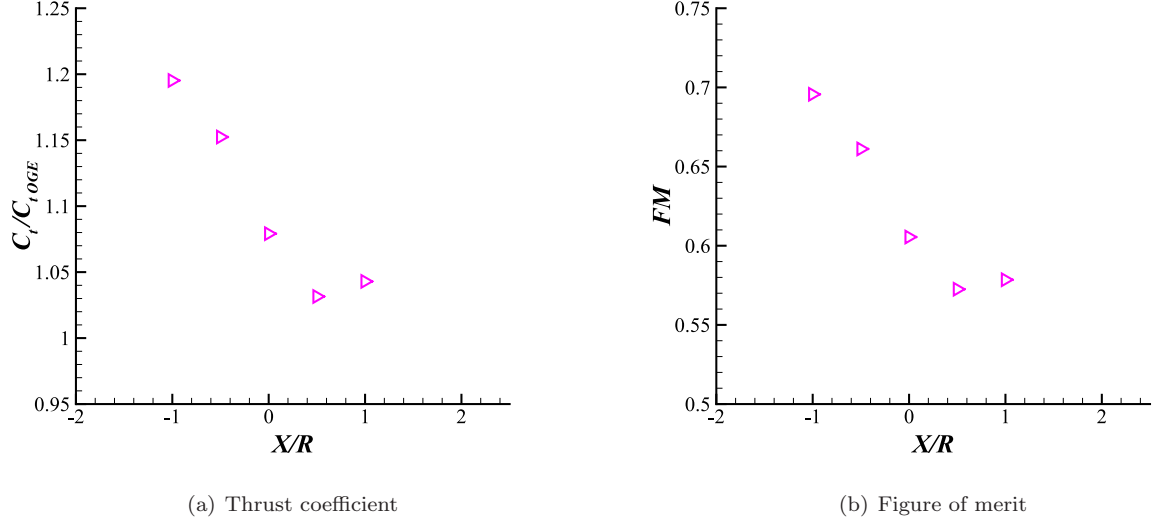
12

(a) Thrust coefficient

(b) Figure of merit

Figure 10: Results of C_t and FM for test 5 (horizontal sweep at $Y/R = 0$, $Z/R = 2$).

4.2 PIV measurements

PIV was used to observe the interacting flow field on the building symmetry plane ahead of the building front face (Fig.5). The PIV measurements were carried out for three different longitudinal positions of the helicopter (X/R = -1, 0, 1) at $Z/R = 2$ and $Y/R = 0$, as given in test 5. Figure 14 presents the velocity field time-averaged over 100 image pairs. The measured flow fields are visualised by means of the in-plane velocity magnitude contours and in-plane streamlines patterns. Figure 15 provides the standard deviation of the in-plane velocity magnitude ($\sigma_{|U|}$) for the same configurations. In general, the considered flows were fairly unsteady, because the average standard deviation was up to 30% of the maximum slipstream velocity (12 m/s).

Figure 14a clearly shows a high-speed layer issued from the roof edge, with the model positioned at X/R = -1. This layer originated from the boundary layer produced by the rotor wake and induced a large recirculating region (clockwise in the figure) ahead of the front face. For $\sigma_{|U|}$, Fig. 15a shows that the most unsteady region corresponded to the wake shear layer, while the region next to the building presented lower values.

For the test condition at $X/R = 0$, just half of the rotor wake impinged the building model roof, as shown by the corresponding pressure pattern of Fig. 13. A clockwise recirculation region produced by the flow blowing from the roof was observed also in this case (Fig. 14b). This recirculation cell was affected by the aft portion of the rotor wake, which was highlighted by the high-velocity slipstream in the top-right corner of the measurement window. For the standard deviation of the in-plane velocity magnitude (Fig. 15b), a substantially different behaviour compared with the previous case was observed. In fact, the region just next to the building model was

characterised by the highest values of $\sigma_{|U|}$. This result confirmed the presence of a highly unsteady structure near the building when the helicopter was hovering on its edge, as pointed out in the previous section on pressure patterns.

A completely different behaviour was observed under the last condition ($X/R = 1$), where the flow topology in the measurement area showed a counterclockwise recirculation region bounded by a high-velocity region corresponding to the rotor fore streamtube boundary (Fig. 14c). The behaviour of the measured flow field was similar to the wake of an isolated rotor under ground effect, as observed by Fradenburgh [18] and Nathan and Green [19]. Similar to the configuration for $X/R = -1$, the highest unsteadiness of the flow field in this case was confined in the shear layer provoked by the high-speed part of the rotor wake, as shown in Figure 15c.

5   CONCLUSIONS

In the present study, a new experimental setup for investigating the aerodynamic interaction between a helicopter and ground obstacles was assessed. The experimental setup basically comprised a motorized helicopter model with a six-component balance and a building model with pressure taps. PIV surveys were carried out in different configurations to clarify the involved flow physics.

First a ground effect test without the building model was conducted in order to produce a set of reference conditions. The results showed very good agreement in terms of C_t with data from past literature for a similar test configuration, which assessed the experimental setup.

A set of tests was then carried out in order to investigate the helicopter–building interference effects. The first test represented a landing on the building roof. The results showed that the beneficial effects in terms of C_t due to interaction with the roof essentially coincided with those of the ground effect, when the rotor projection was entirely on the top of the building. These results demonstrated that a helicopter landing on a surface with dimensions similar to its rotor diameter can expect the same effects as when landing on the ground. Such beneficial effect were reduced for a vertical sweep with the rotor not fully over the building. This feature was confirmed by pressure measurements over the building, where the high-pressure region corresponding to the wake impingement area was not wholly confined to the top of the building. This test showed that a helicopter landing close to the roof edge can expect a ground effect roughly proportional to the extent of the roof area contained in the rotor slipstream. The results of a vertical sweep test performed on the side of the building showed detrimental effects on the thrust coefficient particularly when the rotor was in front of its vertical face. This result showed that even low-rise buildings with a height comparable to the rotor radius may negatively affect the helicopter performance. The pressure patterns revealed overpressures on the side face of the building with the same order of magnitude as those observed on the roof in strong ground effect configurations. Eventually

a test representing an horizontal approach showed a gradual decrease in C_t as the helicopter moved away from the building, because the percentage of the roof inside the slipstream progressively decreased.

This last test was also subject to a PIV survey. A recirculating region, whose topology and morphology were highly dependent on the helicopter position, was found on the side of the building. In particular, the observed flow structure originated from the rotor wake deflection on the upper surface of the building model. For the most external condition that was tested, the typical flow morphology of the ground effect could be observed. When the helicopter was hovering over the edge of the building, a particularly unsteady interaction with the building vertical wall was produced.

C_p scale: -1.5 -0.5 0.5 1.5 2.5 3.5

(a) X/R = -1.07, Y/R = 0, Z/R = 2

(b) X/R = -0.53, Y/R = -0.67, Z/R = 2

(c) X/R = -1.07, Y/R = 0, Z/R = 3

(d) X/R = -0.53, Y/R = -0.67, Z/R = 3

(e) X/R = -1.07, Y/R = 0, Z/R = 4
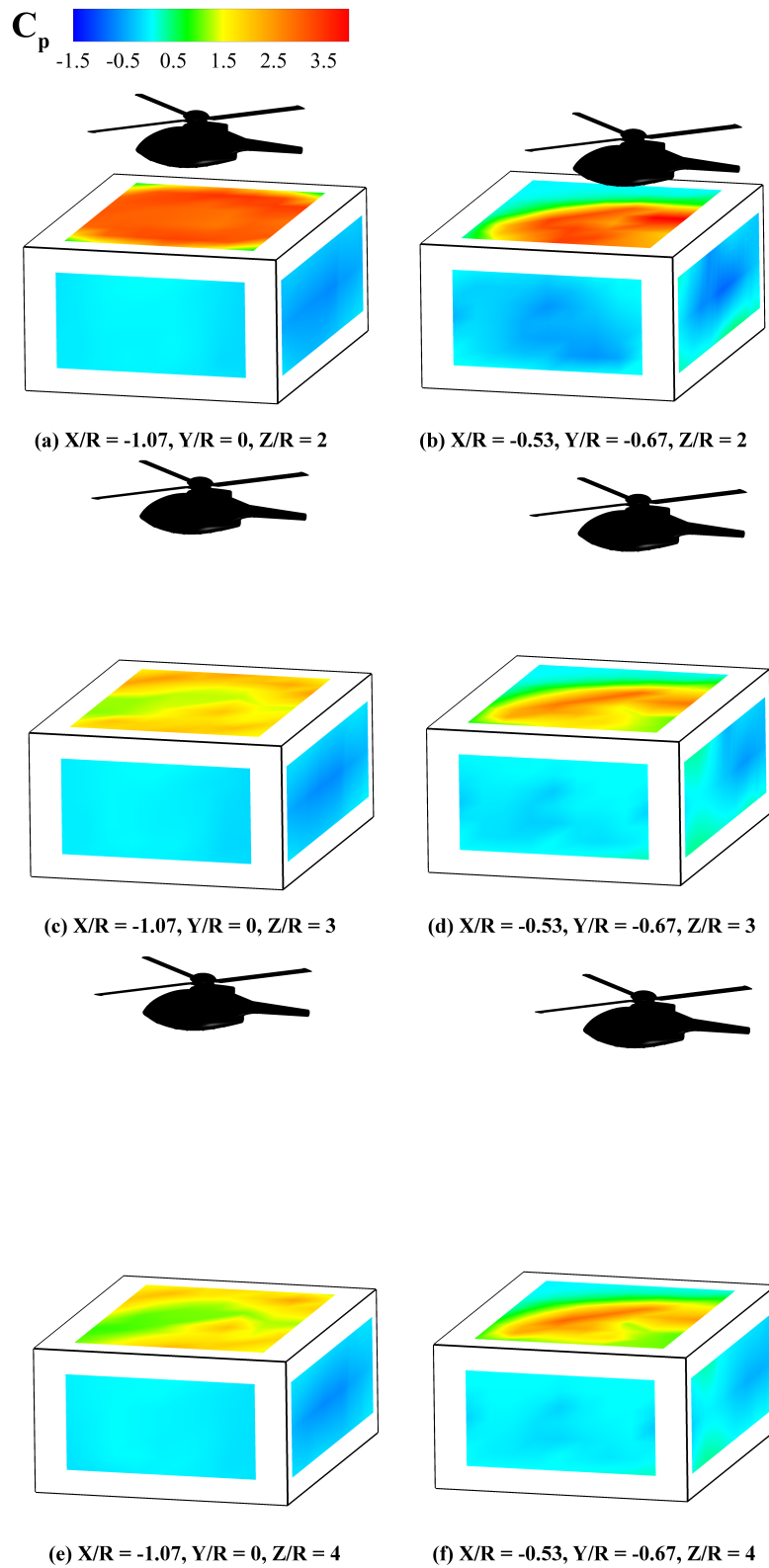
(f) X/R = -0.53, Y/R = -0.67, Z/R = 4

Figure 11: Pressure distribution over the building model under test 2 (left) and test 3 (right) conditions: C_p contours.
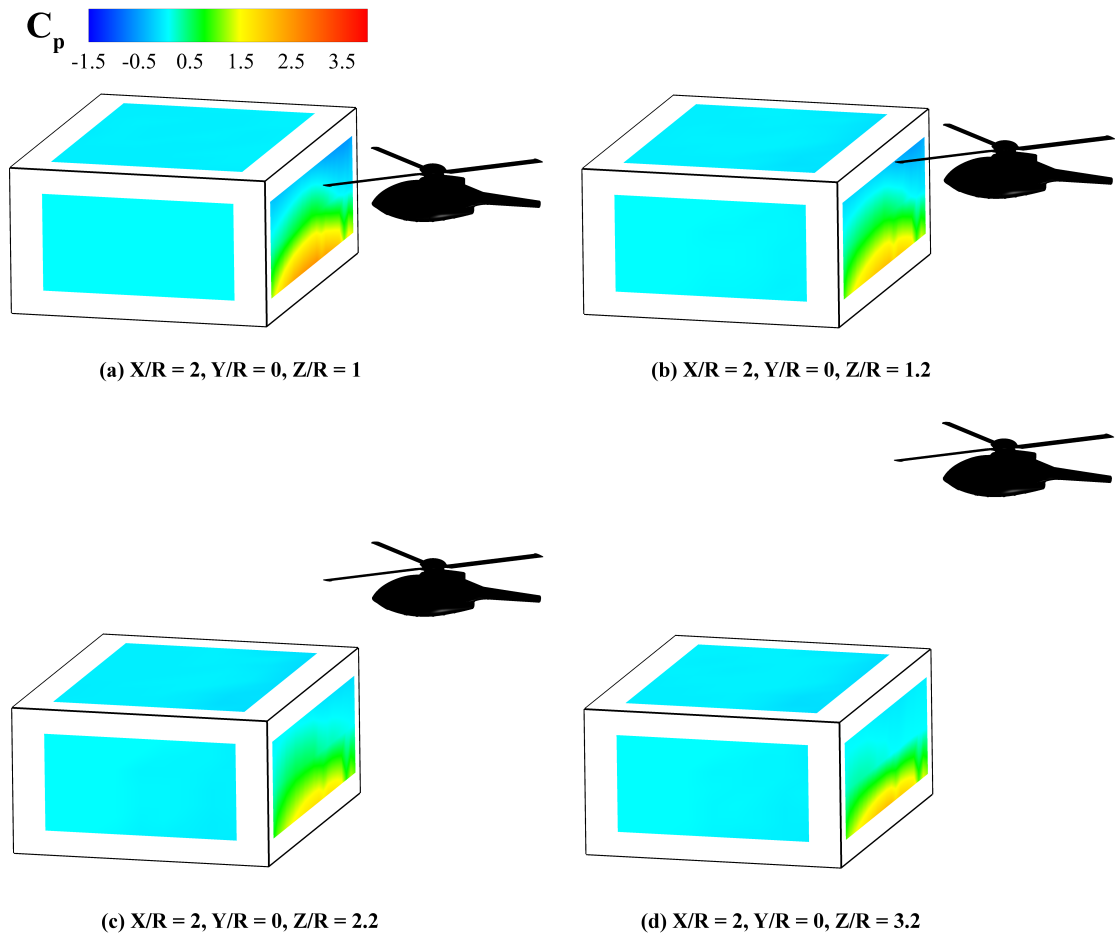
(a) X/R = 2, Y/R = 0, Z/R = 1

(b) X/R = 2, Y/R = 0, Z/R = 1.2

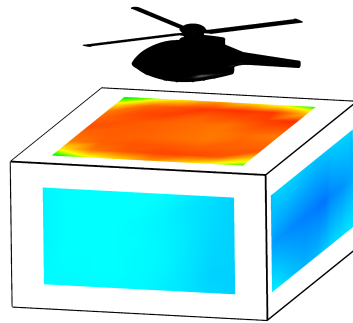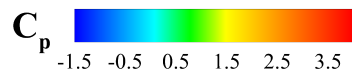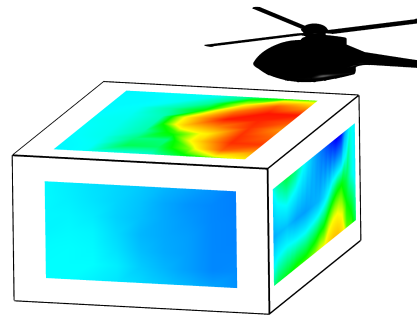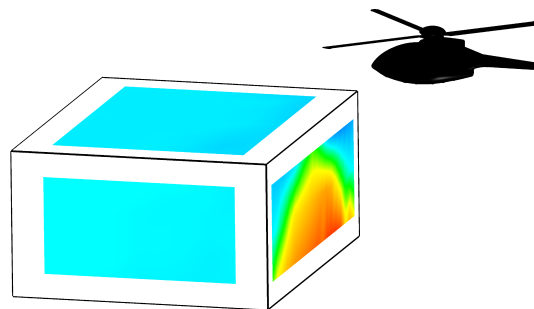(c) X/R = 2, Y/R = 0, Z/R = 2.2

(d) X/R = 2, Y/R = 0, Z/R = 3.2

Figure 12: Pressure distribution over building model under test 4 conditions: C_p contours.
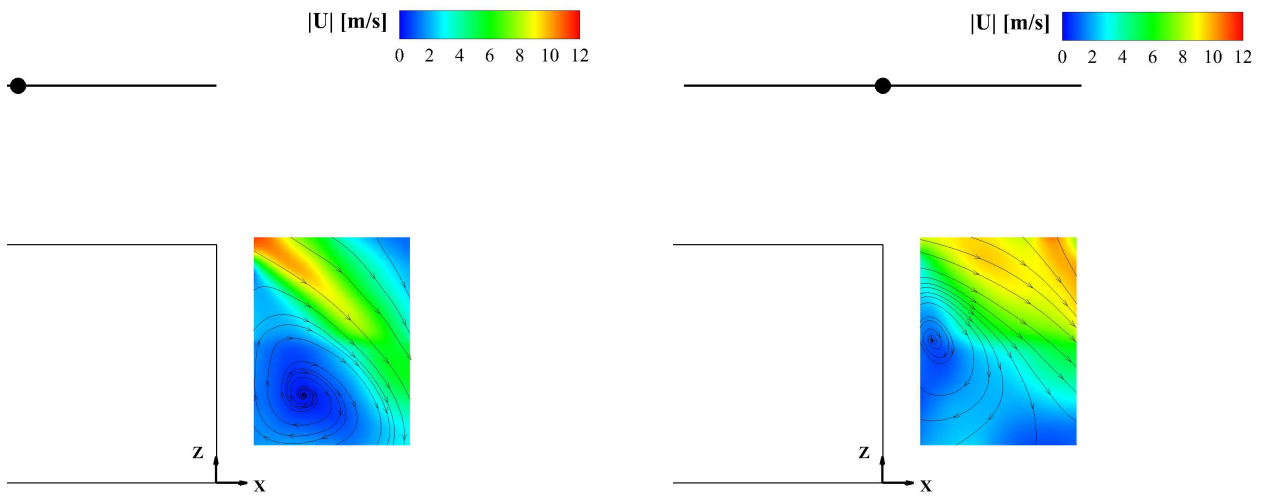
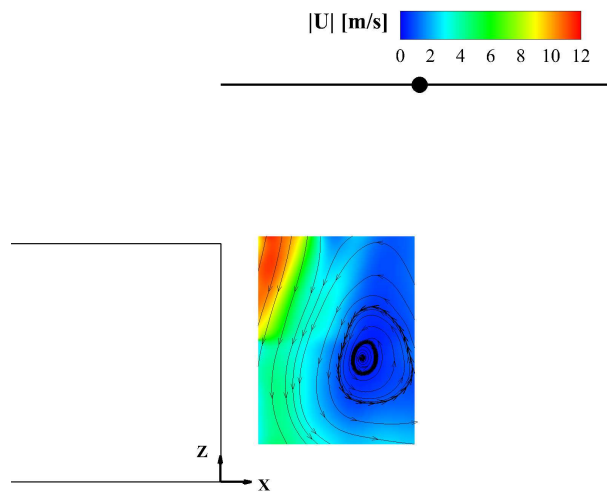(a) X/R = -1, Y/R = 0, Z/R = 2

(b) X/R = 0, Y/R = 0, Z/R = 2

(c) = X/R = 1, Y/R = 0, Z/R = 2

Figure 13: Pressure distribution over building model under test 5 conditions: C_p contours.

(a) $X/R = -1$, $Y/R = 0$, $Z/R = 2$

(b) $X/R = 0$, $Y/R = 0$, $Z/R = 2$

(c) $X/R = 1$, $Y/R = 0$, $Z/R = 2$

Figure 14: PIV results for test 5 conditions: velocity magnitude contours and in-plane streamlines.
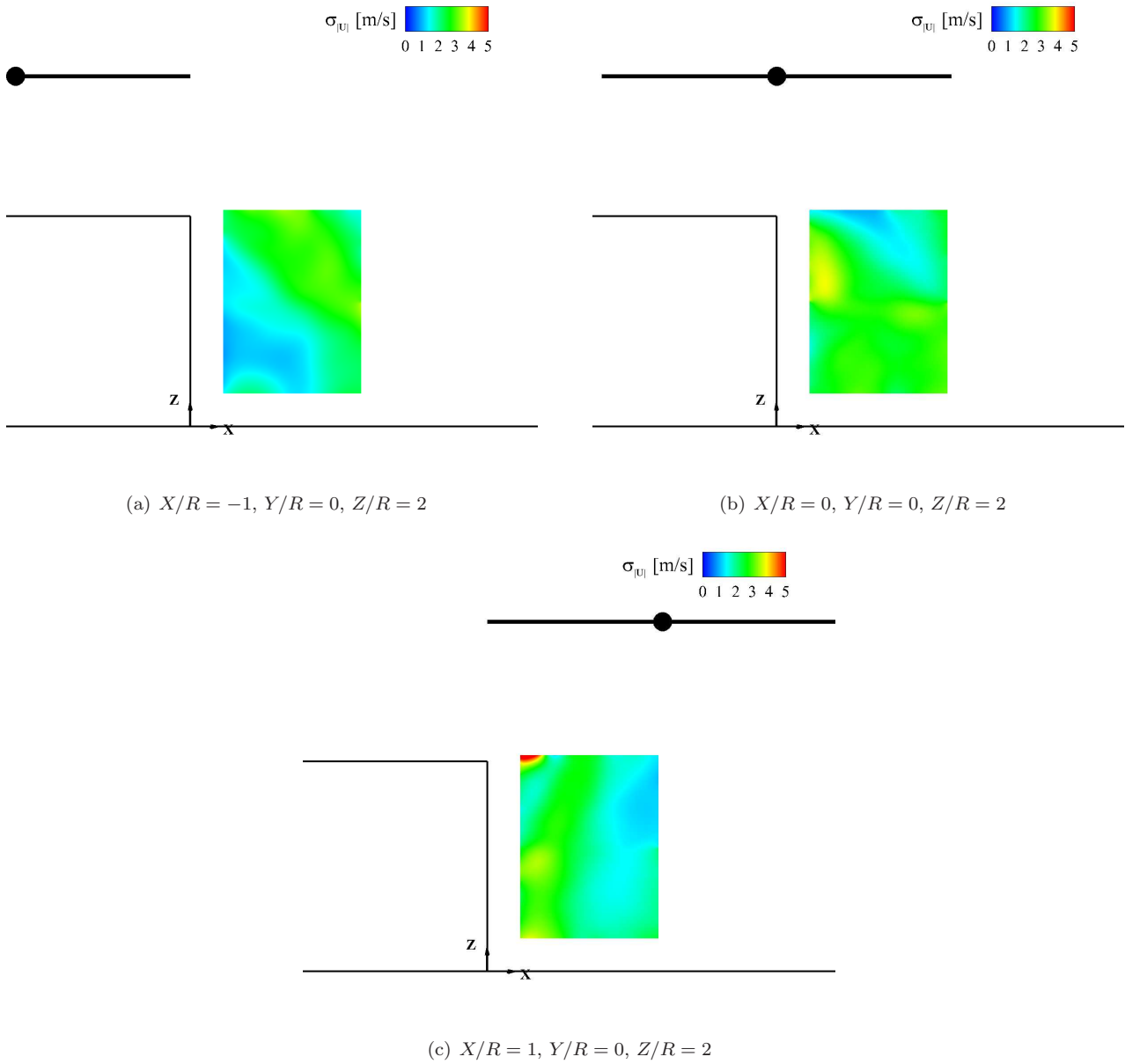
(a) $X/R = -1$, $Y/R = 0$, $Z/R = 2$

(b) $X/R = 0$, $Y/R = 0$, $Z/R = 2$

(c) $X/R = 1$, $Y/R = 0$, $Z/R = 2$

Figure 15: PIV results for test 5 conditions: contours of standard deviation of in-plane velocity magnitude.

APPENDIX

Nomenclature

A	rotor area
c	blade section model chord
CFD	Computational Fluid Dynamics
C_p	pressure coefficient
C_t	thrust coefficient, $\equiv \frac{T}{\rho V_{TIP}^2 A}$
C_q	torque coefficient, $\equiv \frac{Q}{\rho V_{TIP}^2 AR}$
DLR	German Aerospace Center
FAA	Federal Aviation Administration
FM	Figure of Merit $\equiv \frac{C_t^{3/2}}{C_q\sqrt{2}}$
IGE	In Ground Effect
IHST	International Helicopter Safety Team
JHSAT	Joint Helicopter Safety Analysis Team
M	Mach number
MT	Momentum Theory
OGE	Out of Ground Effect
P_∞	far-field Pressure
PIV	Particle Image Velocimetry
R	rotor radius
RPM	revolutions per minute
Re_{TIP}	Reynolds number at the blade tip, $\equiv \frac{V_{\text{TIP}}c}{\nu}$
$|U|$	velocity magnitude
$\sigma_{|U|}$	standard deviation of the velocity magnitude
V_{TIP}	tip blade speed, $\equiv \Omega R$
V_{IND}	Rotor induced velocity
X	longitudinal coordinate
Y	span-wise coordinate
Z	vertical coordinate

References

[1] International Helicopter Safety Team. The U.S. JHSAT Baseline of Helicopter Accident Analysis, www.ihst.org/portals/54/US_JSHAT_Compendium_Report1.pdf, 2011.

[2] Federal Aviation Administration. Helicopter Flying Handbook, FAA-H-8083-21A, USA, 2012

[3] Crozon C, Steijl R and Barakos G.N. Numerical Studies of Rotors in Ship Airwake, *39th European Rotorcraft Forum*, Moscow, 3-6 September 2013.

[4] Alpman E, Long LN, Bridges DO and Horn JH. Fully-Coupled Simulations of the Rotorcraft / Ship Dynamic Interface, *AHS International 63rd Annual Forum & Technology Display*, Virginia Beach, VA, USA, 1-3 May 2007.

[5] Timm GK. Obstacle-Induced Flow Recirculation, *Journal of the American Helicopter Society* 1965; 10:1-5.

[6] Lee RG and Zan SJ. Wind Tunnel Testing of a Helicopter Fuselage and Rotor in a Ship Airwake, *29th European Rotorcraft Forum*, Friedrichshafen, Germany, 16-18 September 2003.

[7] Lee RG and Zan SJ. Wind Tunnel Testing to Determine Unsteady Loads on a Helicopter Fuselage in a Ship Airwake, *23rd International Congress of Aeronautical Sciences*, Toronto, Canada, 8-13 September 2002.

[8] Zan SJ. Experimental determination of rotor thrust in a ship airwake. *Journal of the American Helicopter Society*, 47(2), 100-108, 2002.

[9] Nacakli Y and Landman D. Helicopter Downwash/Frigate Airwake Interaction Flowfield PIV Surveys in a Low Speed Wind Tunnel, *AHS International 67th Annual Forum & Technology Display*, Virginia Beach, VA, USA, 3-5 May 2011.

[10] Rajagopalan G, Niazi S, Wadcock AJ, Yamauchi GK and Silva MJ. Experimental and computational Study of the Interaction Between a Tandem-Rotor Helicopter and a Ship, *American Helicopter Society 61st Annual Forum*, Gravepine, TX, USA, 1-3 June 2005.

[11] Quinliven TA and Long KR. Rotor Performance in the Wake of a Large Structure, *American Helicopter Society 61st Annual Forum*, Gravepine, TX, USA, 1-3 June 2005.

[12] Polsky SA and Wilkinson CH, A Computational Study of Outwash for a Helicopter Operating Near a Vertical Face with Comparison to Experimental Data, *AIAA Modeling and Simulation Technologies Conference*, Chicago, IL, USA, 10-13 August 2009.

[13] Pahlke K. GARTEUR Helicopter Cooperative Research, *36th European Rotorcraft Forum*, Paris, France, 7-9 September 2010.

[14] Polak DR, Werner R and Albert RG. Effects of an image plane on the tiltrotor fountain flow. *Journal of the American Helicopter Society*, 45(2), 90-96, 2000.

[15] Polak DR and George AR. (1998). Flowfield and acoustic measurements from a model tiltrotor in hover, *Journal of aircraft*, 35(6), 921-929, 1998.

[16] PIVview 2C version 3.0, User Manual, PIVTEC, www.pivtec.com.

[17] Leishman J. Principles of helicopter aerodynamics. *Cambridge University Press* 2006.

[18] Fradenburgh EA. The helicopter and the ground effect machine. *Journal of the American Helicopter Society*, 5(4): 24-33, 1960.

[19] Nathan ND and Green RB. The flow around a model helicopter main rotor in ground effect. *Experiments in fluids*, 52(1): 151-166. 2012.